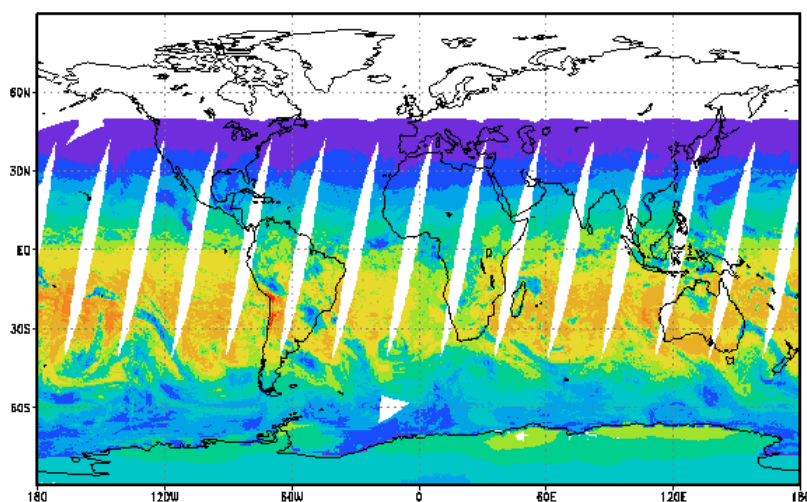


O3M SAF VALIDATION REPORT

Validated products:

Identifier	Name
O3M-30 ... O3M-31	Offline daily maximum photolysis rates
O3M-93 ... O3M-94	Offline UV D-vitamin weighting
O3M-95... O3M-109	Metop-B Offline UV products



Authors:

Name	Institute
Niilo Kalakoski, Jukka Kujanpää	Finnish Meteorological Institute

Reporting period: O3M-30: March 2008 – September 2008
 O3M-93... O3M-94: June 2007 - September 2012
 O3M-95... O3M-109: June 2012 – May 2013

Input data versions: NTO/O3 version GDP 4.6
 MetOp-A AVHRR L1b LAC version 1.0, since 1 June 2007
 MetOp-B AVHRR L1b LAC version 1.0, since 10 April 2013
 N-18 AVHRR L1b GAC version 0.0, since 1 June 2007
 N-18 AVHRR L1b GAC version 1.0, since 20 September 2007
 N-19 AVHRR L1b GAC version 1.0, since 3 June 2009

Data processor versions: OUV processor version 1.20

Introduction to EUMETSAT Satellite Application Facility on Ozone and Atmospheric Chemistry Monitoring (O3M SAF)

Background

The need for atmospheric chemistry monitoring was first realized when severe loss of stratospheric ozone was detected over the Polar Regions. At the same time, increased levels of ultraviolet radiation were observed.

Ultraviolet radiation is known to be dangerous to humans and animals (causing e.g. skin cancer, cataract, immune suppression) and having harmful effects on agriculture, forests and oceanic food chain. In addition, the global warming - besides affecting the atmospheric chemistry - also enhances the ozone depletion by cooling the stratosphere. Combined, these phenomena have immense effects on the whole planet. Therefore, monitoring the chemical composition of the atmosphere is a very important duty for EUMETSAT and the world-wide scientific community.

Objectives

The main objectives of the O3M SAF is to process, archive, validate and disseminate atmospheric composition products (O₃, NO₂, SO₂, OClO, HCHO, BrO, H₂O), aerosols and surface ultraviolet radiation utilising the satellites of EUMETSAT. The majority of the O3M SAF products are based on data from the GOME-2 spectrometer onboard MetOp-A satellite.

Another important task of the O3M SAF is the research and development in radiative transfer modelling and inversion methods for obtaining long-term, high-quality atmospheric composition products from the satellite measurements.

Product families

- Near real-time Total Column (NTO)
 - O₃, NO₂, SO₂, O₃Tropo, NO₂Tropo
- Near real-time Ozone Profile (NOP)
- Near real-time UV Index (NUV)
- Offline Total Column (OTO)
 - O₃, NO₂, O₃Tropo, NO₂Tropo, SO₂, BrO, H₂O, HCHO, OClO
- Offline Ozone Profile (OOP)
- Offline Surface UV (OUV)
- Aerosols (ARS)

Product timeliness and dissemination

Data products are divided in two categories depending on how quickly they are available to users:

Near real-time products are available in less than three hours after measurement. These products are disseminated via EUMETCast (NTO, NOP), GTS (NTO, NOP) or Internet (NUV).

Offline products are available in two weeks from the measurement and they are archived at the O3M SAF archives in Finnish Meteorological Institute (OOP, OUV, ARS) and German Aerospace Center (OTO).

Only products with “pre-operational” or “operational” status are disseminated. Up-to-date status of the products and ordering info is available on the O3M SAF website.

Information about the O3M SAF project, products and services: <http://o3msaf.fmi.fi/>

O3M SAF Helpdesk: o3msaf@fmi.fi

Document change log

Issue	Date	Modified items
1/2013 draft	28.5.2013	Initial version
1/2014	14.1.2014	Modified according to ORR for the CDOP-2 Metop-B products and PCR/ORR for the photolysis rate (backlog) and vitamin D RIDS and subsequent discussions. Added comparison figures for weighting functions other than CIE. Added clarification of differences in GOME-2A/B comparisons. Photolysis rate terminology corrected. Removed $j(\text{NO}_2)$ comparisons. Typos fixed.
2/2014	5.11.2014	Added new $j(\text{NO}_2)$ comparisons (sect. 2.3).
2/2014	21.11.2014	Re-organized the photolysis rate comparison sections.
2/2014	3.2.2015	Screening of the ground-based data clarified (p.28).

Contents

1	Introduction	1
1.1	Purpose and scope	1
1.2	Acronyms	1
1.3	References	1
1.3.1	Applicable Documents	1
1.3.2	Reference Documents	1
2	Validation results	2
2.1	GOME-2B products	2
2.2	Photolysis rates	23
2.2.1	O ₃ photolysis rates	24
2.2.2	NO ₂ photolysis rates	25
2.3	Vitamin D weighting function	30
3	Conclusions	31

Chapter 1

Introduction

1.1 Purpose and scope

The purpose of this document is to present the validation of EUMETSAT Satellite Application Facility on Atmospheric Chemistry Monitoring (O3M SAF) Offline UV products, specifically photolysis rates, D-vitamin weighted daily doses and maximum dose rates and GOME-2B products.

1.2 Acronyms

ATBD	Algorithm Theoretical Basis Document
CIE	Commission Internationale de L'Eclairage, International Commission on Illumination
EUMETSAT	European Organisation for the Exploitation of Meteorological Satellites
FMI	Finnish Meteorological Institute
GOME	Global Ozone Monitoring Experiment
O3M SAF	Satellite Application Facility on Ozone and Atmospheric Chemistry Monitoring
OUV	Offline UV product

1.3 References

1.3.1 Applicable Documents

- [AD1] OUV Algorithm Theoretical Basis Document, SAF/O3M/FMI/ATBD/001, Issue 1.4, 28.6.2013.
- [AD2] OUV Products User Manual, SAF/O3M/FMI/PUM/001, Issue 1.5, 28.6.2013.
- [AD3] O3M SAF Product Requirements Document, Hovila, J., S. Kiemle, O. Tuinder, H. Joench-Soerensen, F. Karcher

1.3.2 Reference Documents

- [RD1] Zaveri, R.A., Shaw, W.J. and Cziczo, D.J., "CARES: Carbonaceous Aerosol and Radiative Effects Study Science Plan", May 2010, DOE/SC-ARM-10-017, <http://www.arm.gov/publications/programdocs/doe-sc-arm-10-017.pdf?id=65>

Chapter 2

Validation results

2.1 GOME-2B products

GOME-2B daily dose and daily maximum dose rate products were currently available for only one day, April 10th 2013. Figures 2.1 - 2.15 show maps from GOME-2A and GOME-2B, difference (GOME-2B - GOME-2A) and relative difference ($100 * [\text{GOME-2B} - \text{GOME-2A}] / \text{GOME-2B}$) for this day for all OUV products. Median values of differences and relative differences as a function of latitude are shown in the figures 2.16 - 2.30. Median relative differences are less than 3 % in almost all the cases but can reach up to 25 % at high solar zenith angles for some products.

While generally differences between two instruments are within expected range, products show some cyclical differences. These are seen especially in daily dose products in mid-latitudes and in Solar noon UV index product at equator. These differences are most likely due to the differences in cloud modelling as a result of 50 minute difference in orbits of Metop-A and B. This causes differences in observation geometry. Products are affected differently since different AVHRR instrument (aboard Metop or NOAA satellites) overpasses are used in cloud detection depending on time and location of the overpass and the specific OUV product. For further information on choice of input data, see ATBD.

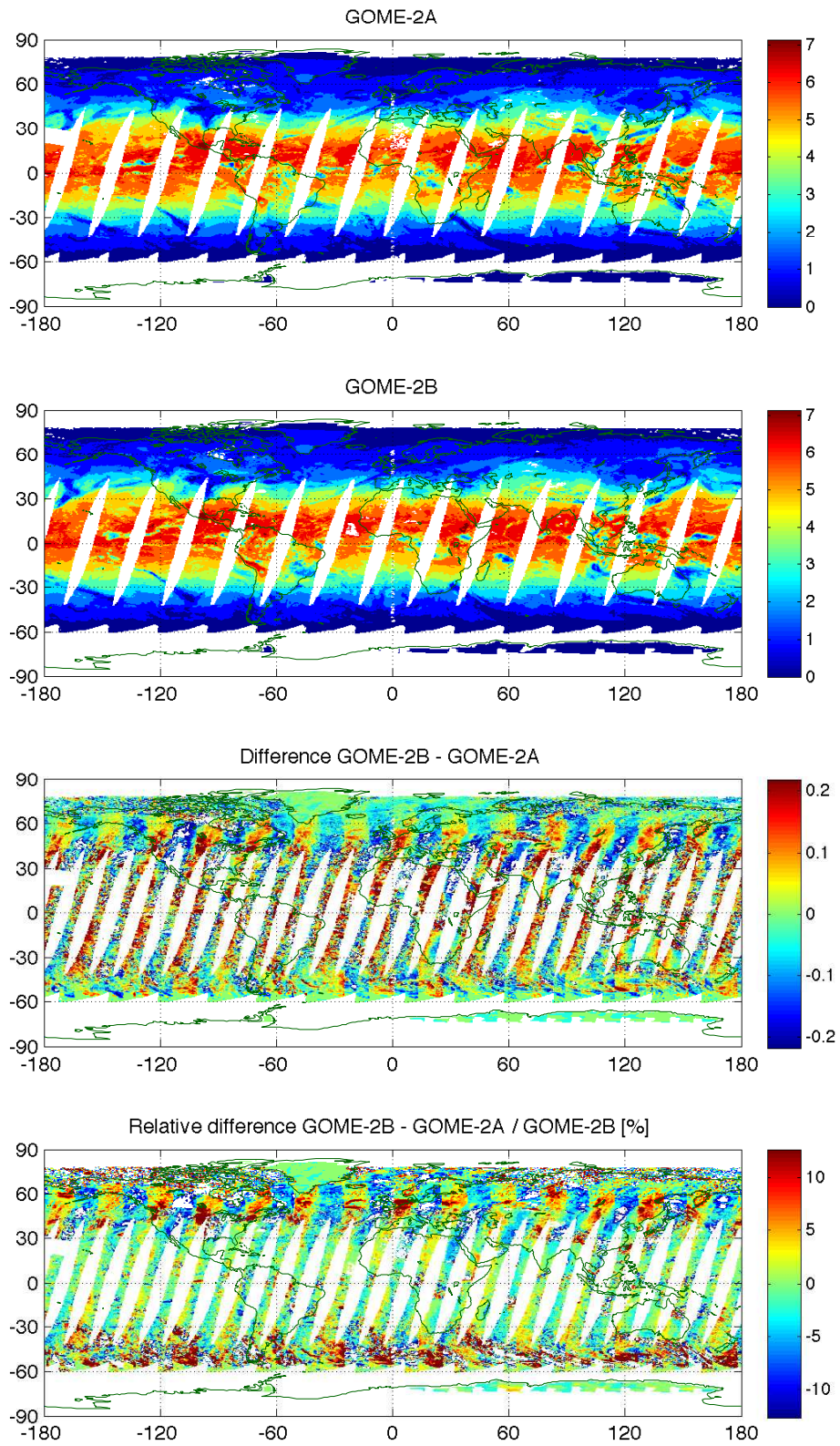


Figure 2.1: CIE weighted daily dose for 10.4.2013. GOME-2A(top), GOME-2B (second), absolute difference (third) and relative difference (bottom).

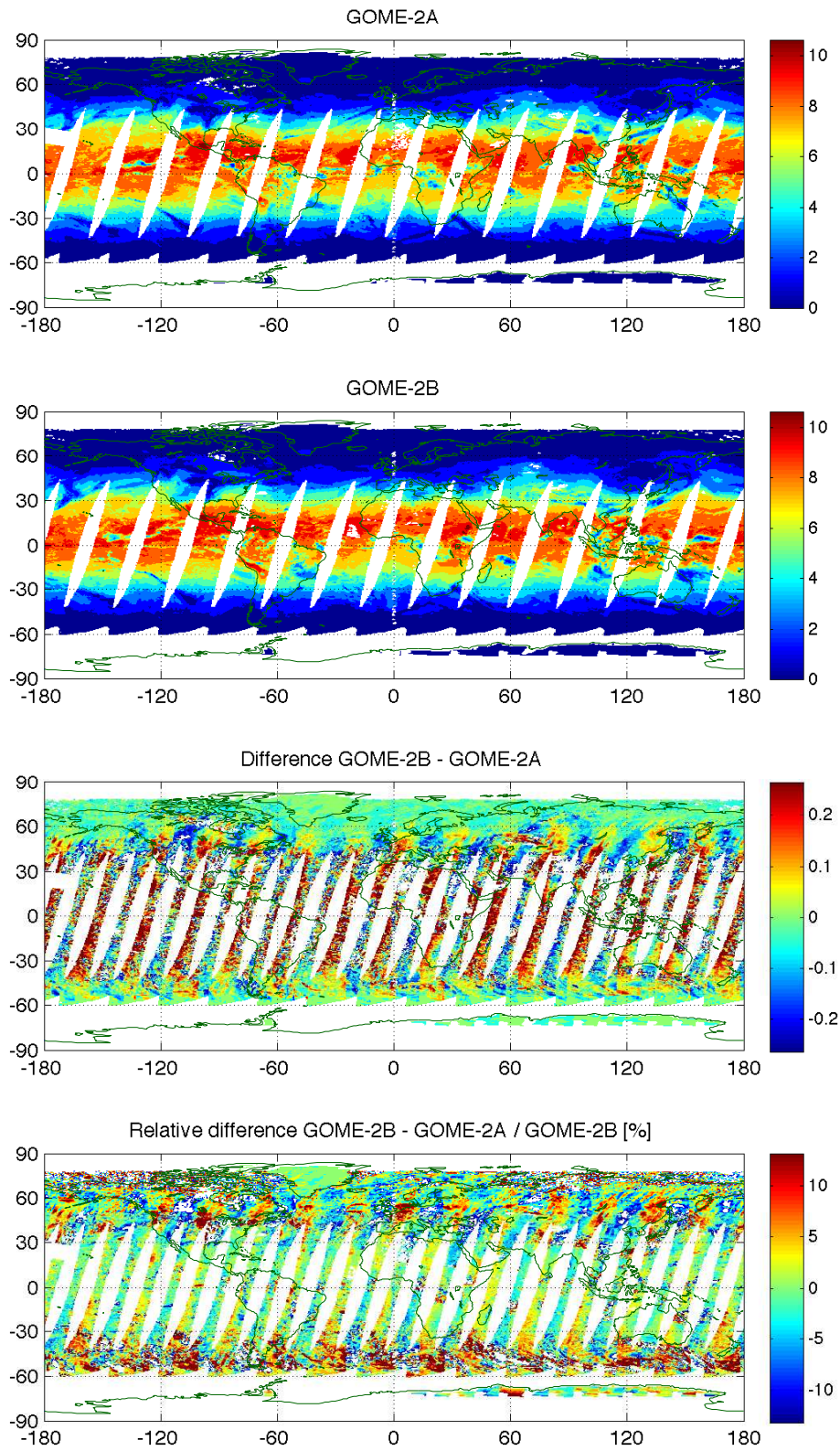


Figure 2.2: Plant response weighted daily dose for 10.4.2013. GOME-2A(top), GOME-2B (second), absolute difference (third) and relative difference (bottom).

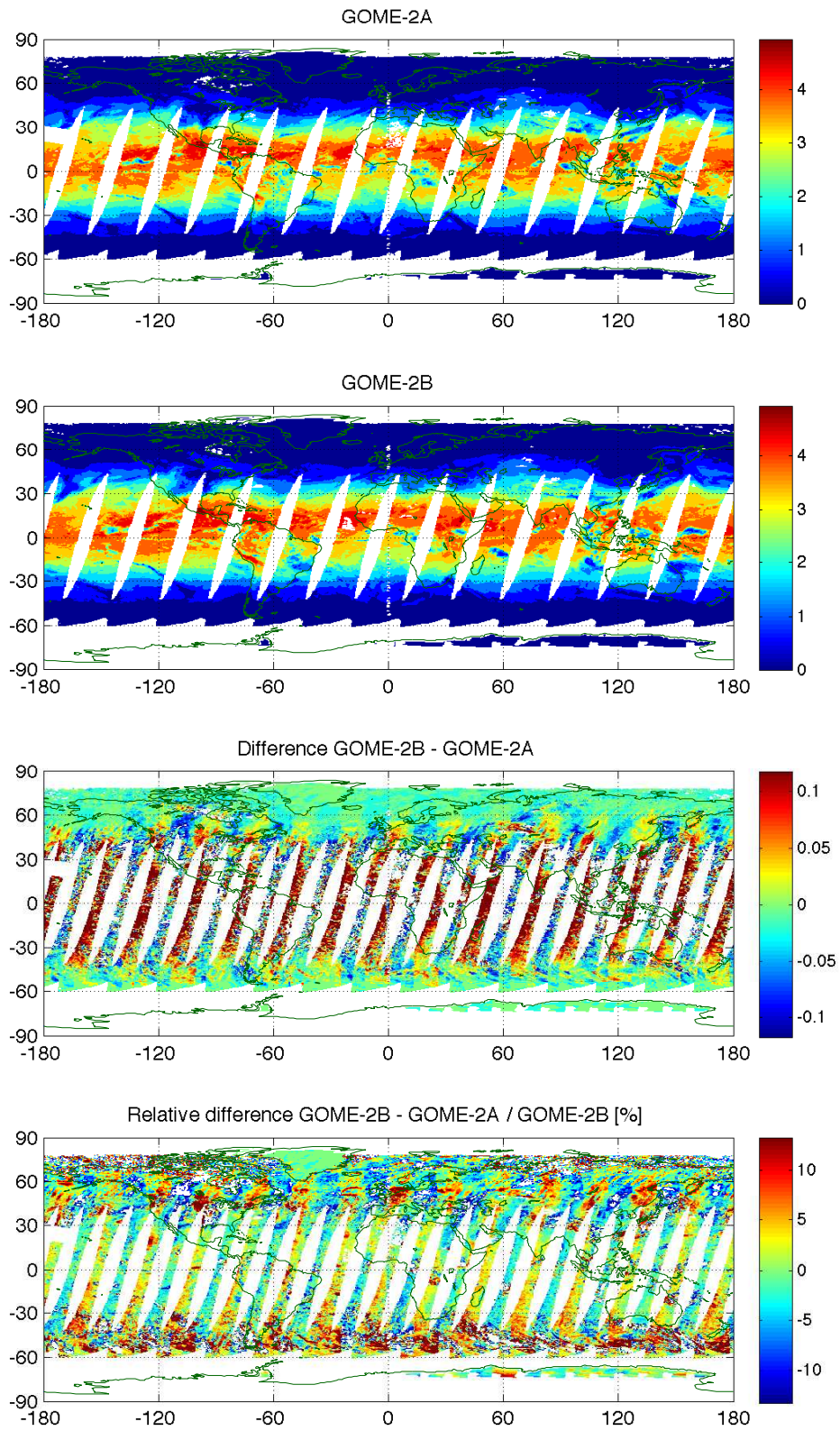


Figure 2.3: DNA damage weighted daily dose for 10.4.2013. GOME-2A(top), GOME-2B (second), absolute difference (third) and relative difference (bottom).

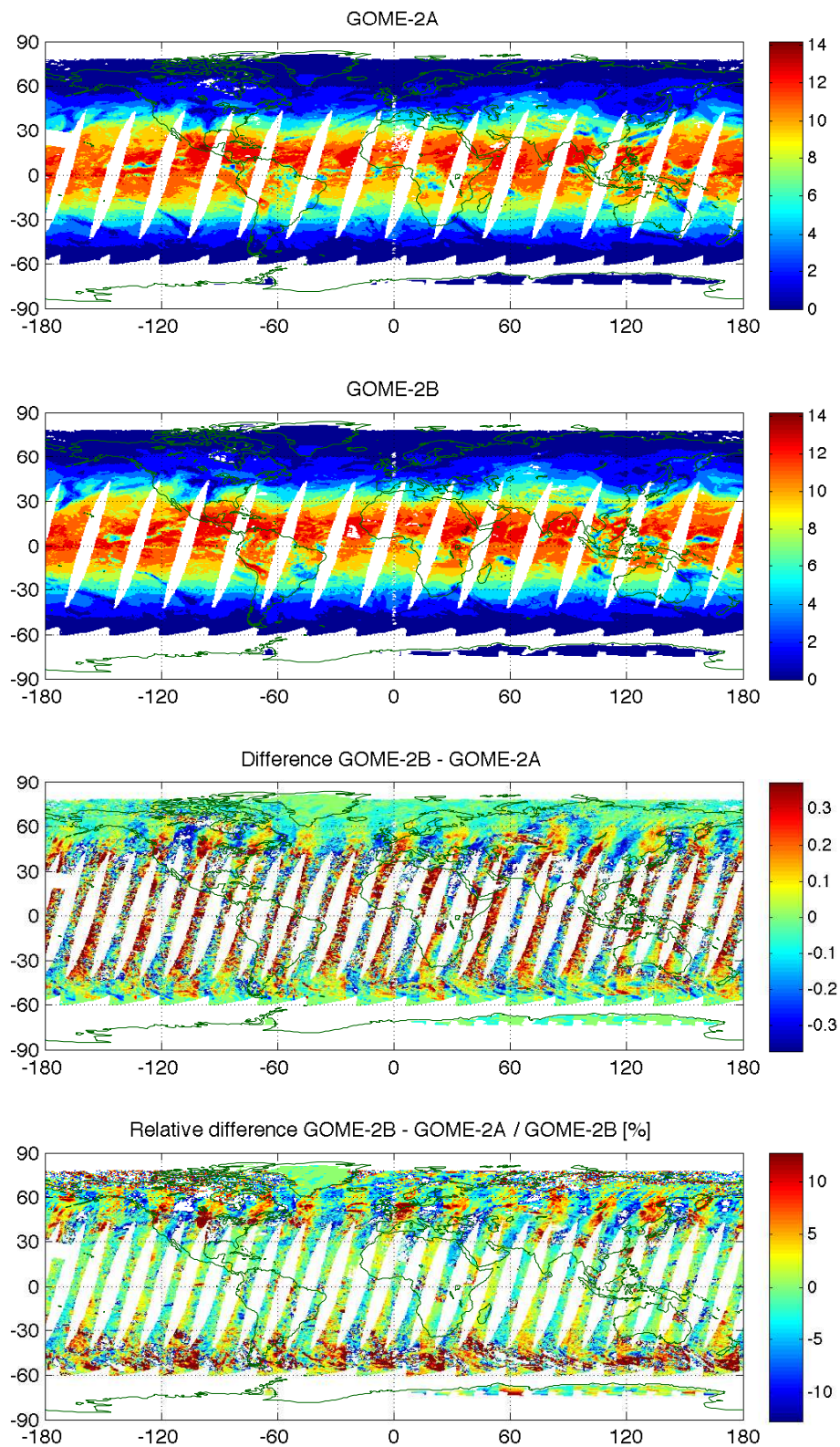


Figure 2.4: Vitamin D weighted daily dose for 10.4.2013. GOME-2A(top), GOME-2B (second), absolute difference (third) and relative difference (bottom).

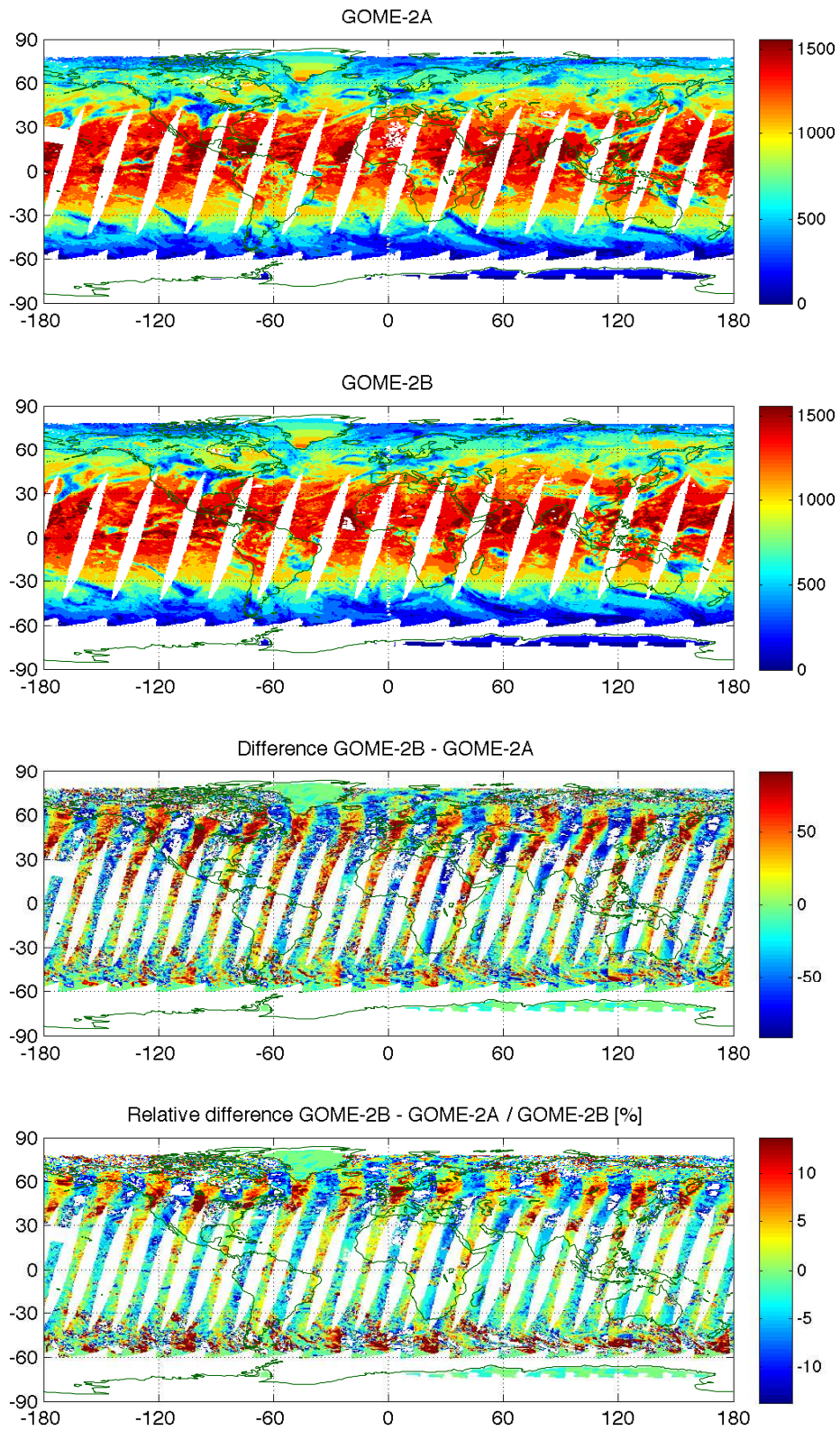


Figure 2.5: UVA weighted daily dose for 10.4.2013. GOME-2A(top), GOME-2B (second), absolute difference (third) and relative difference (bottom).

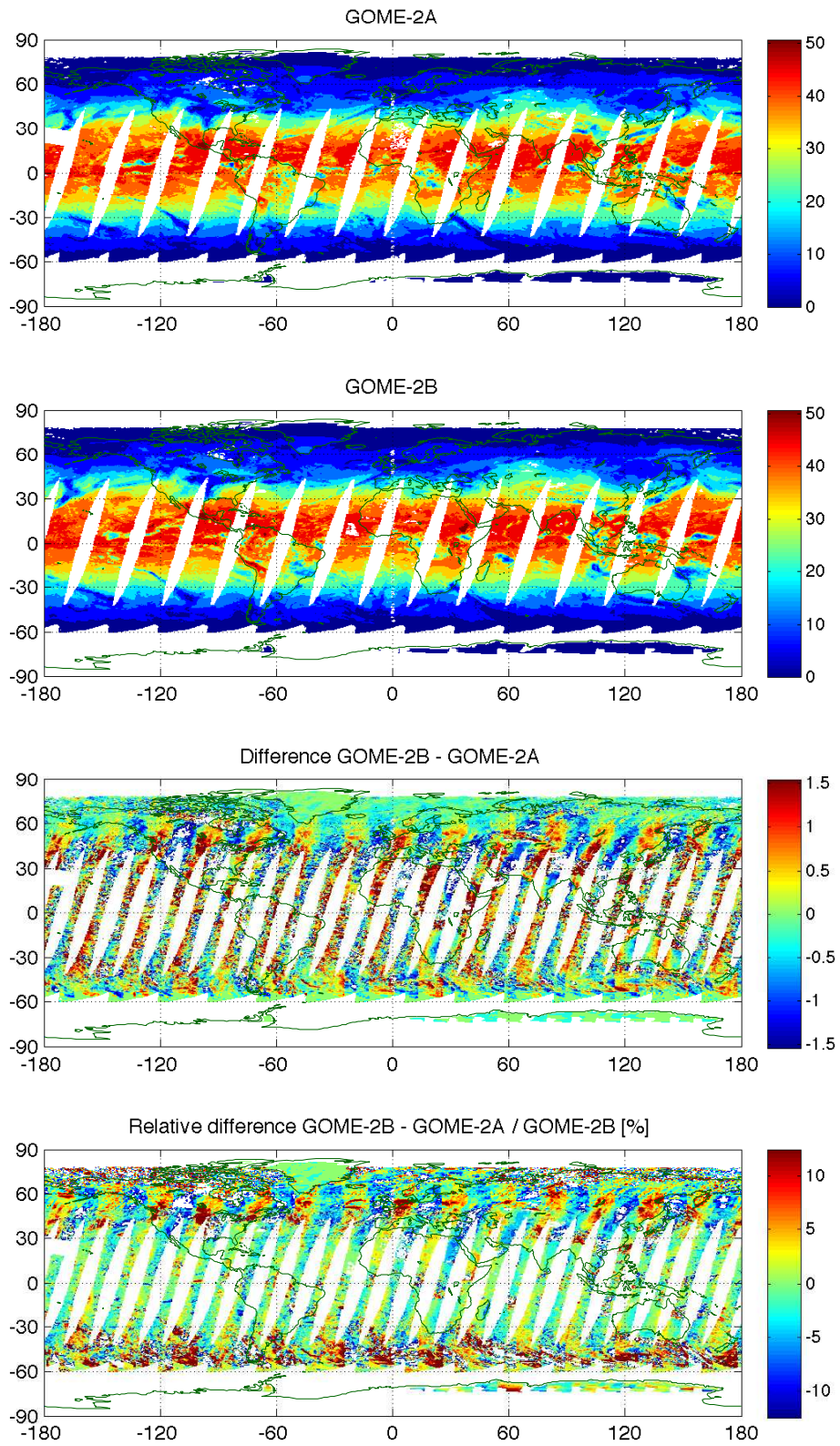


Figure 2.6: UVB weighted daily dose for 10.4.2013. GOME-2A(top), GOME-2B (second), absolute difference (third) and relative difference (bottom).

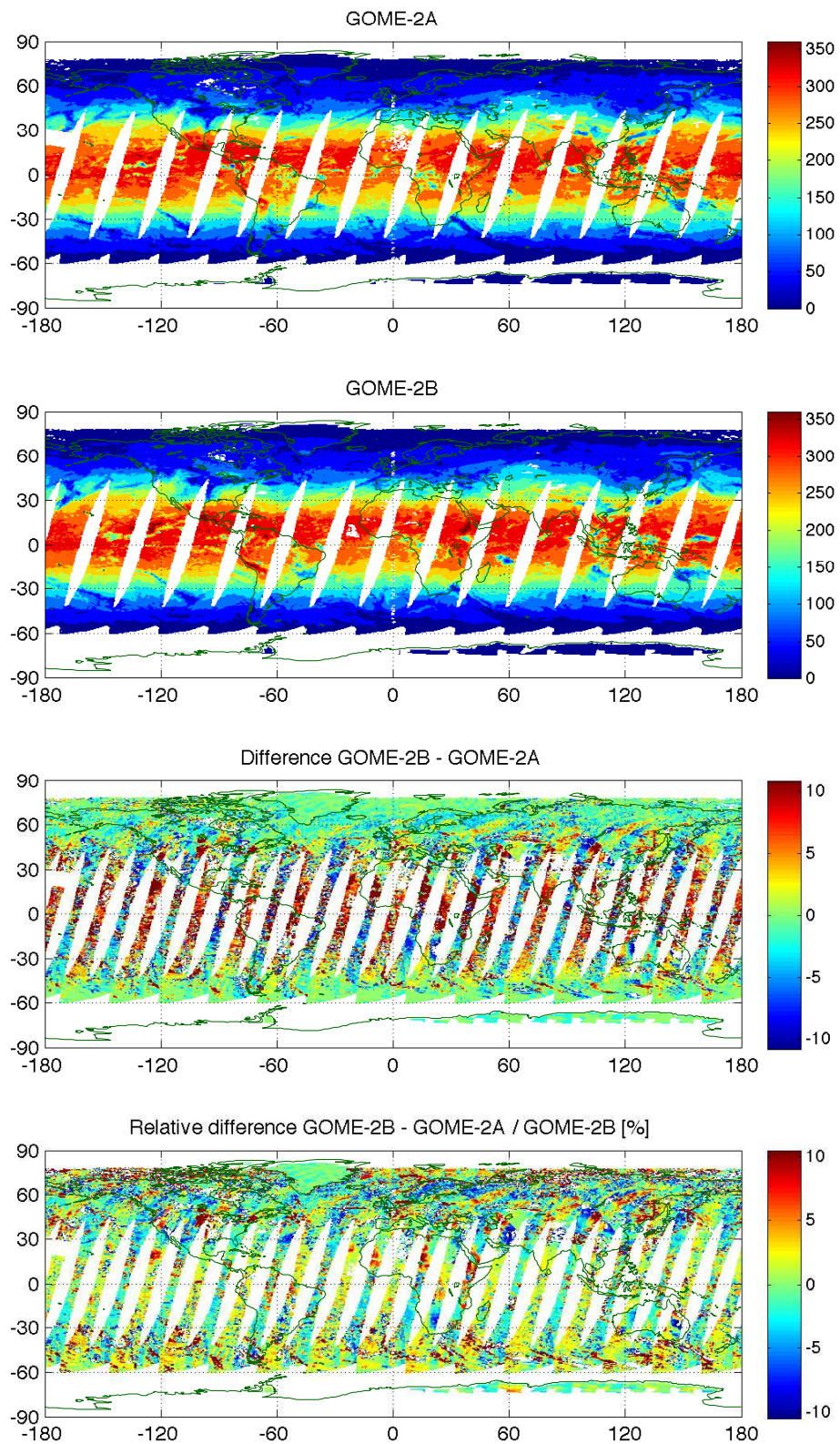


Figure 2.7: CIE weighted daily maximum dose rate for 10.4.2013. GOME-2A(top), GOME-2B (second), absolute difference (third) and relative difference (bottom).

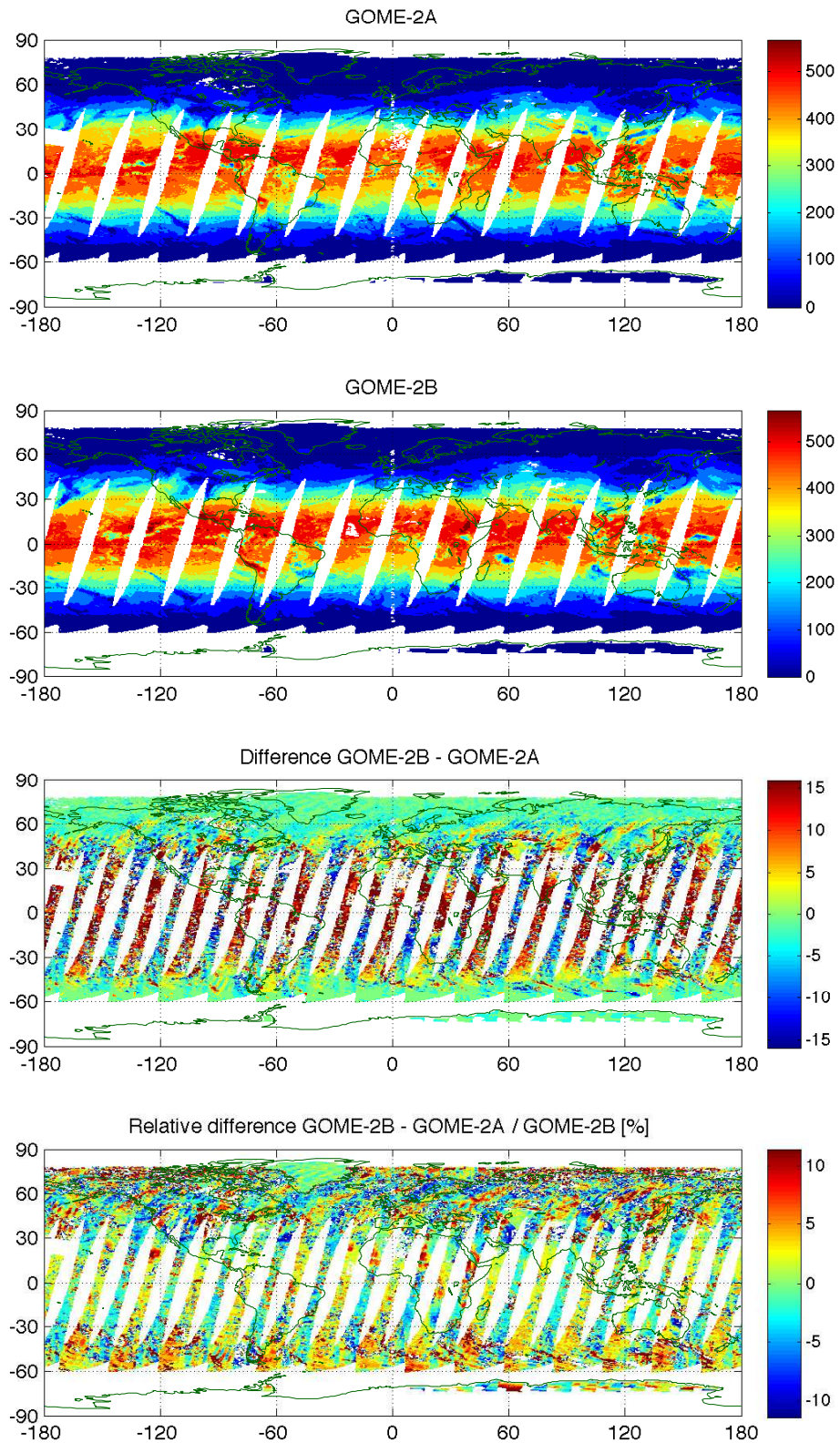


Figure 2.8: Plant response weighted daily maximum dose rate for 10.4.2013. GOME-2A(top), GOME-2B (second), absolute difference (third) and relative difference (bottom).

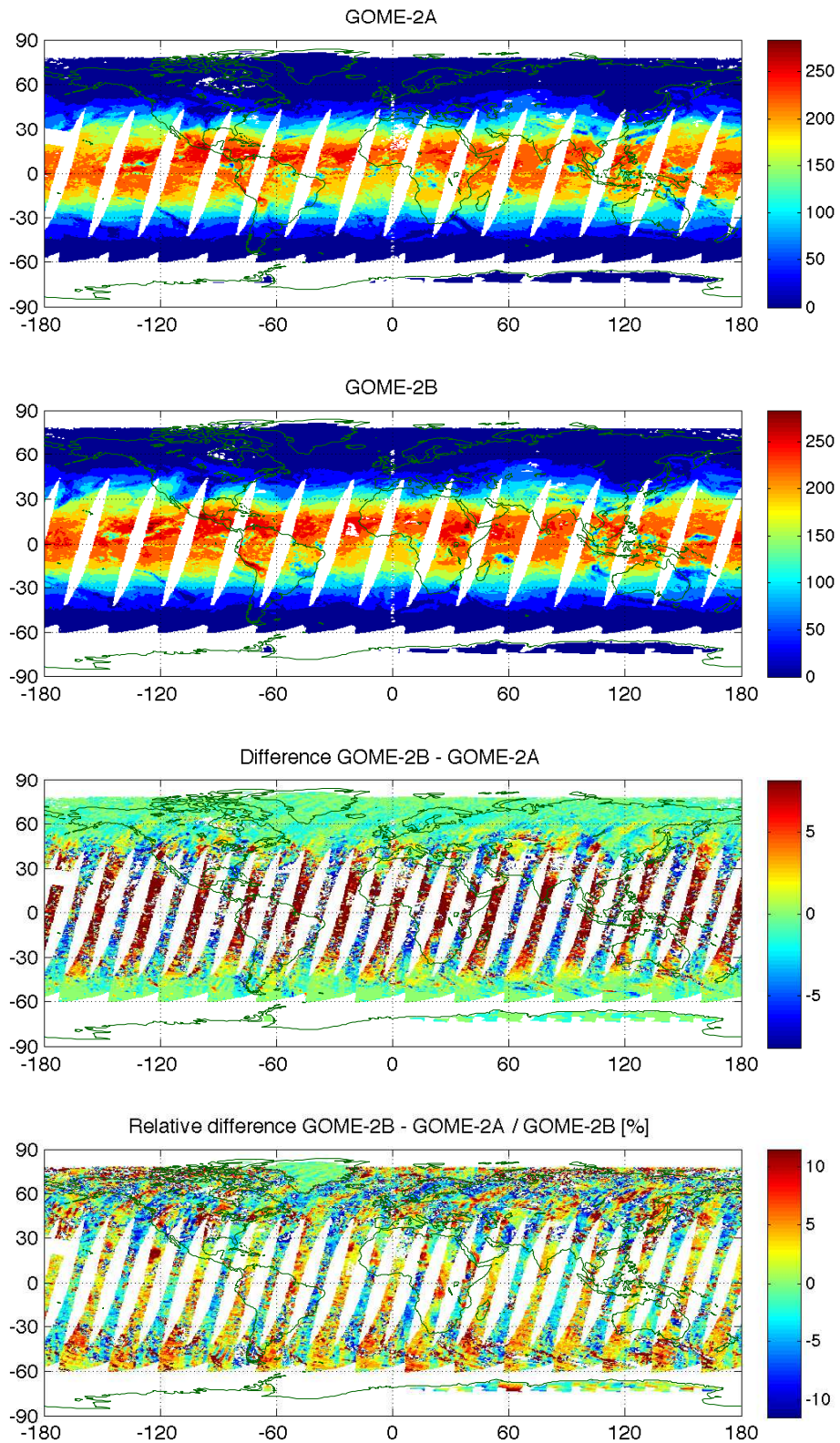


Figure 2.9: DNA damage weighted daily maximum dose rate for 10.4.2013. GOME-2A(top), GOME-2B (second), absolute difference (third) and relative difference (bottom).

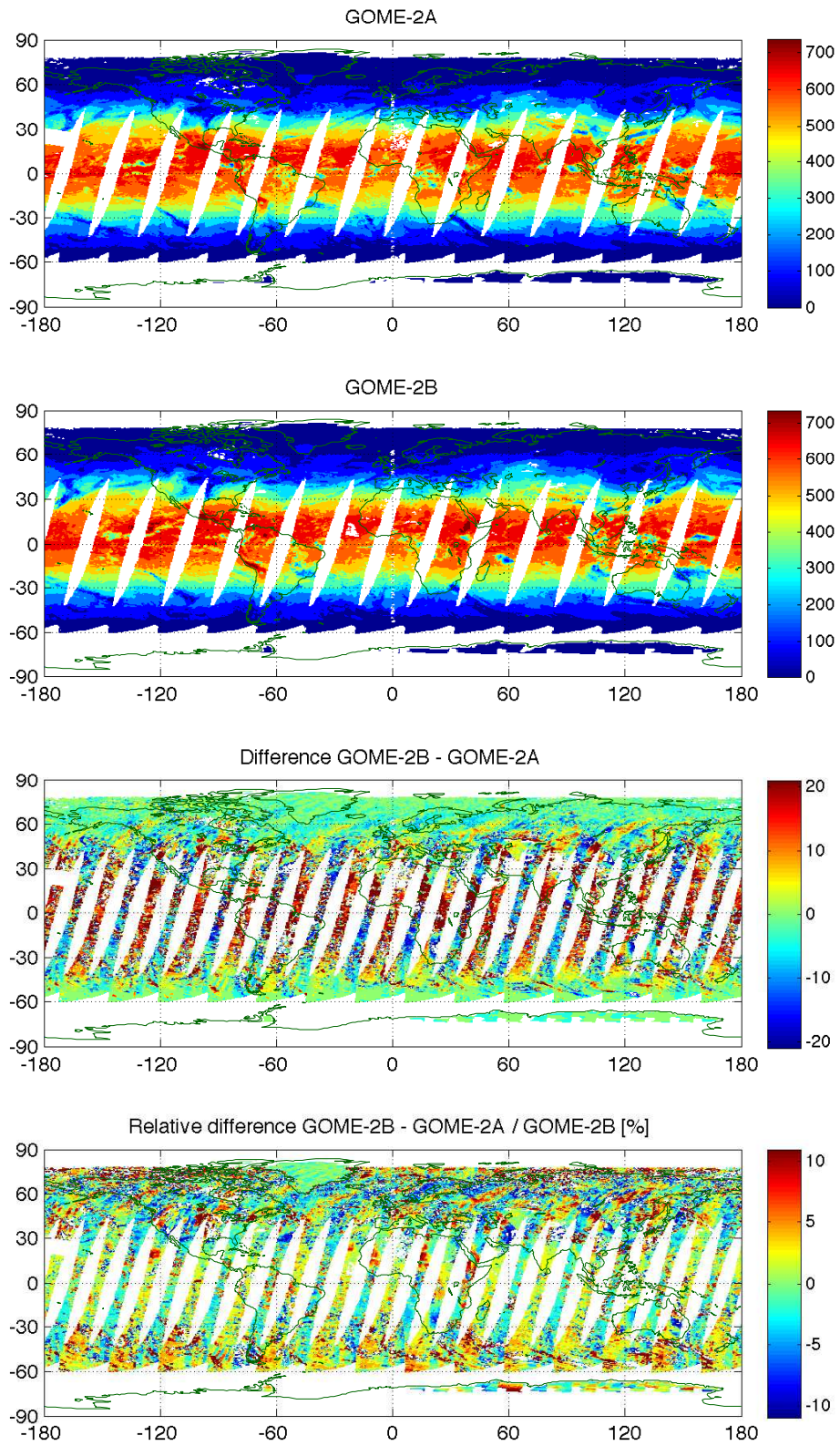


Figure 2.10: Vitamin D weighted daily maximum dose rate for 10.4.2013. GOME-2A(top), GOME-2B (second), absolute difference (third) and relative difference (bottom).

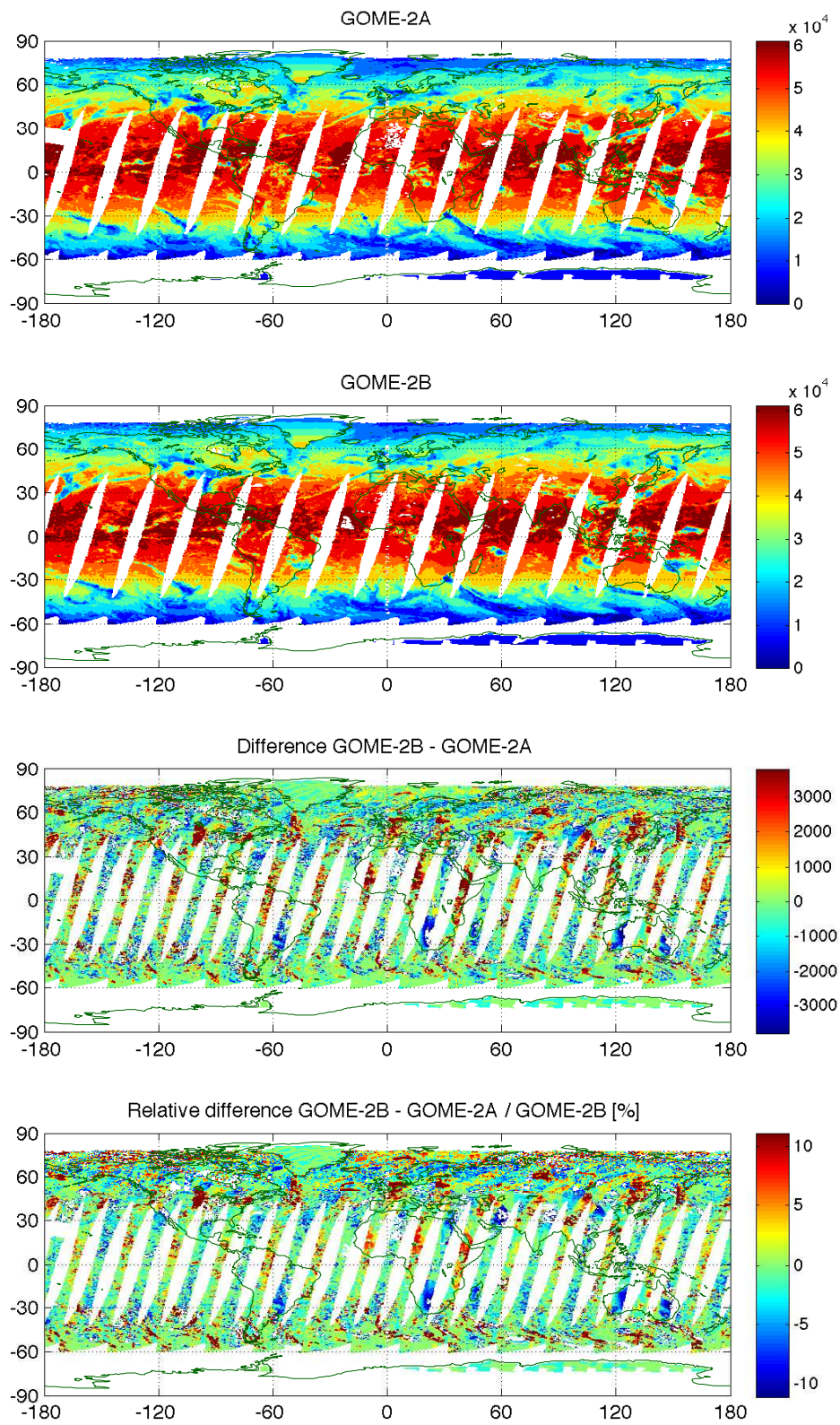


Figure 2.11: UVA weighted daily maximum dose rate for 10.4.2013. GOME-2A(top), GOME-2B (second), absolute difference (third) and relative difference (bottom).

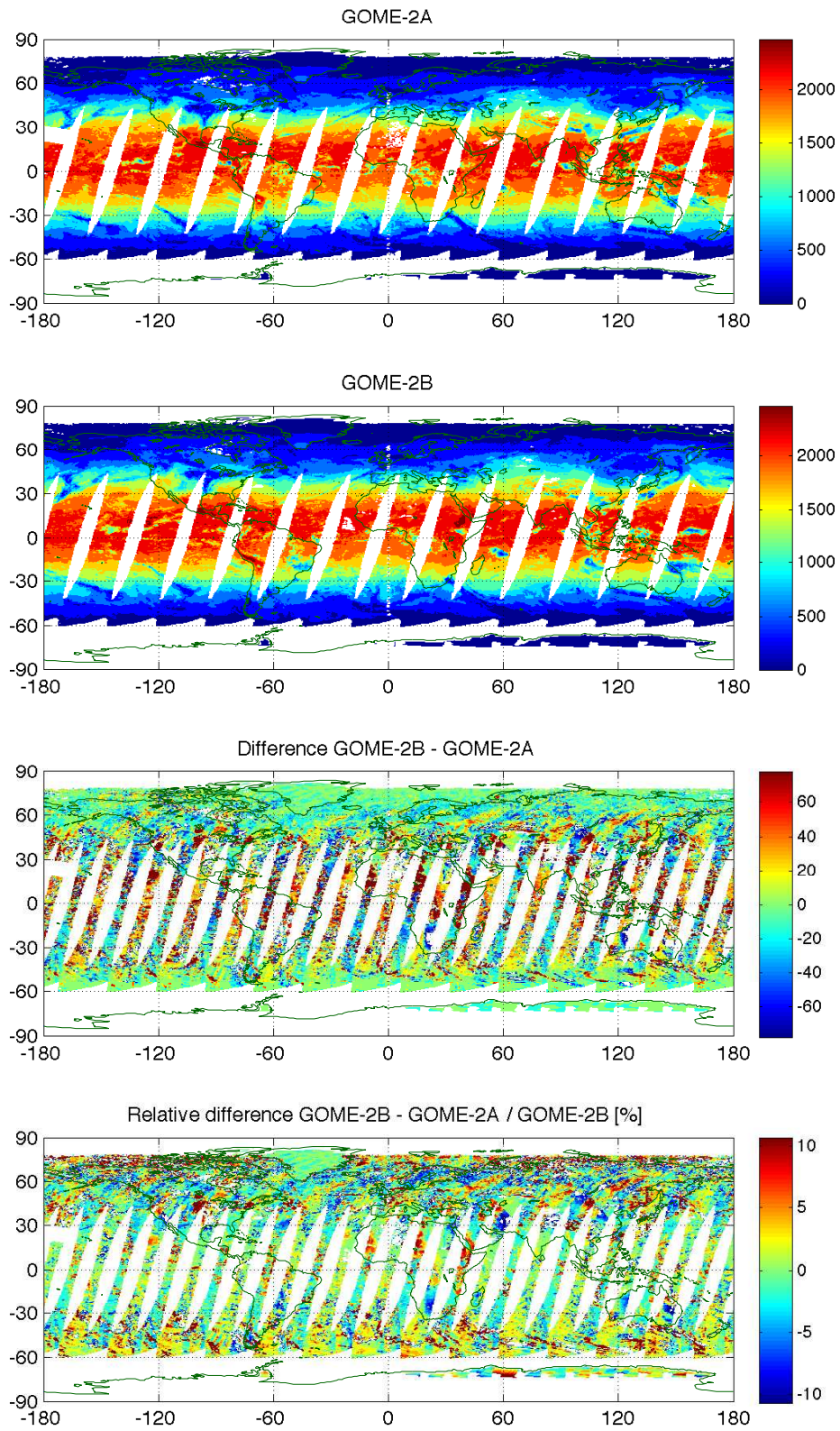


Figure 2.12: UVB weighted daily maximum dose rate for 10.4.2013. GOME-2A(top), GOME-2B (second), absolute difference (third) and relative difference (bottom).

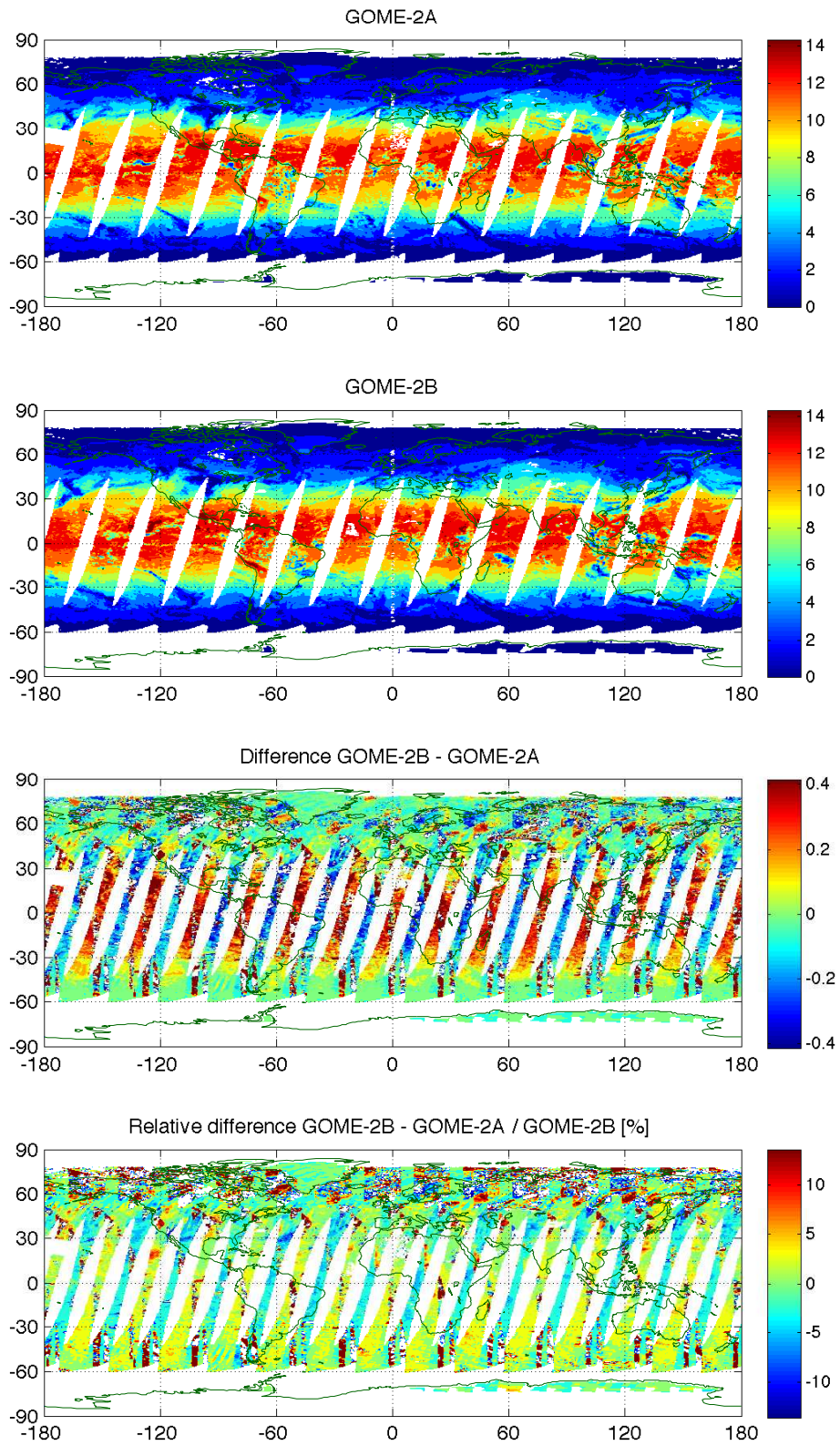


Figure 2.13: Solar noon UV index for 10.4.2013. GOME-2A(top), GOME-2B (second), absolute difference (third) and relative difference (bottom).

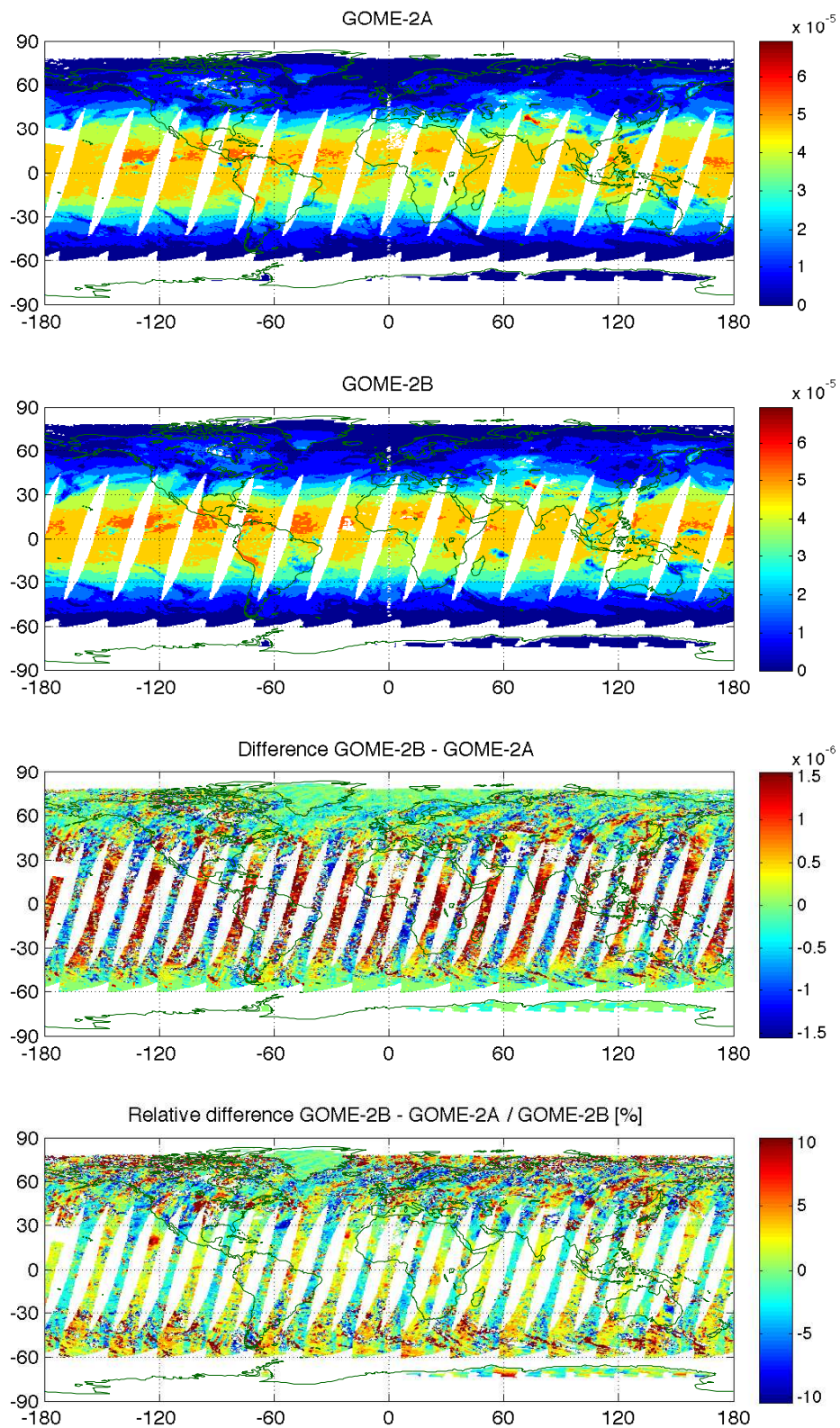


Figure 2.14: Daily maximum ozone photolysis rate for 10.4.2013. GOME-2A(top), GOME-2B (second), absolute difference (third) and relative difference (bottom).

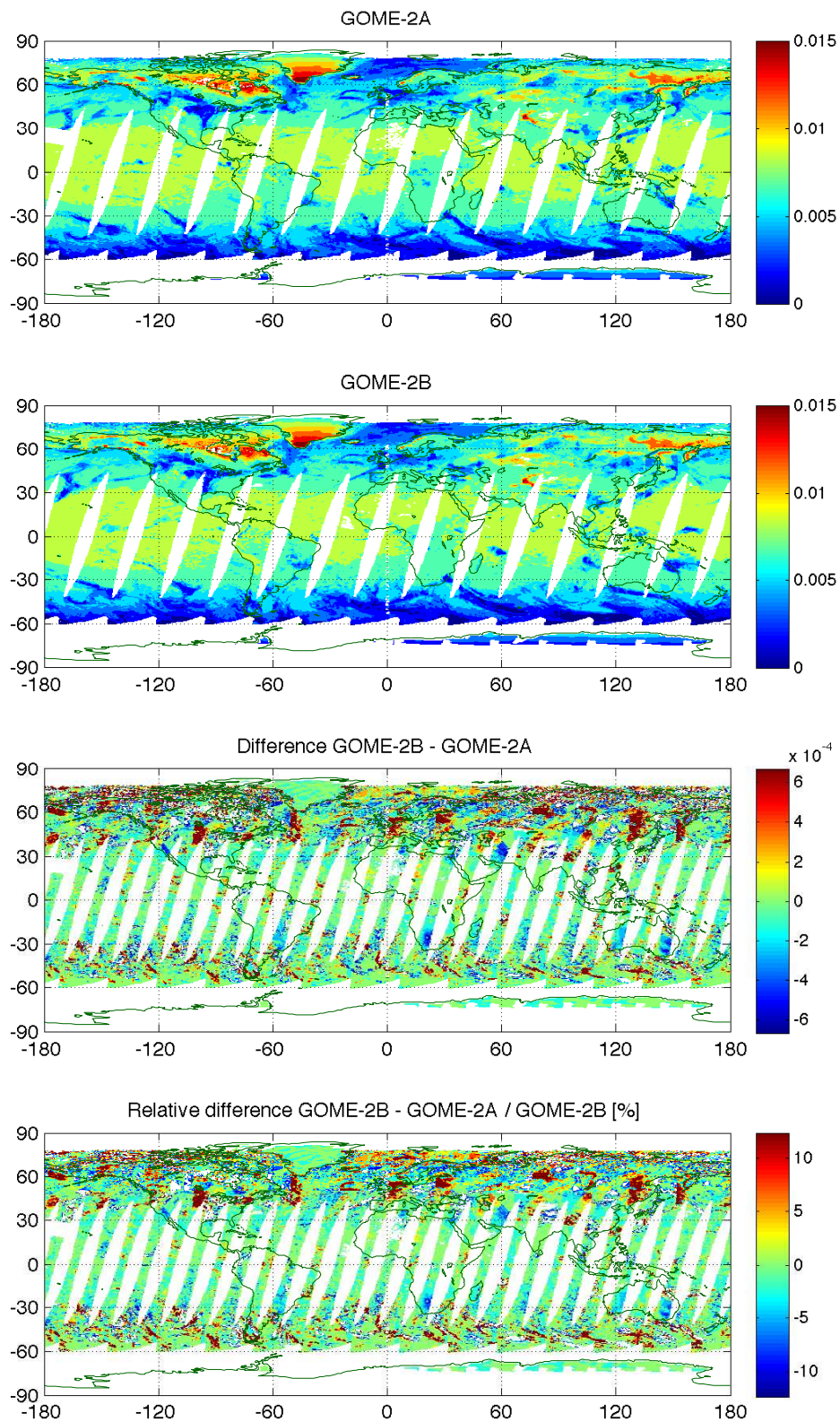


Figure 2.15: Daily maximum NO₂ photolysis rate for 10.4.2013. GOME-2A(top), GOME-2B (second), absolute difference (third) and relative difference (bottom).

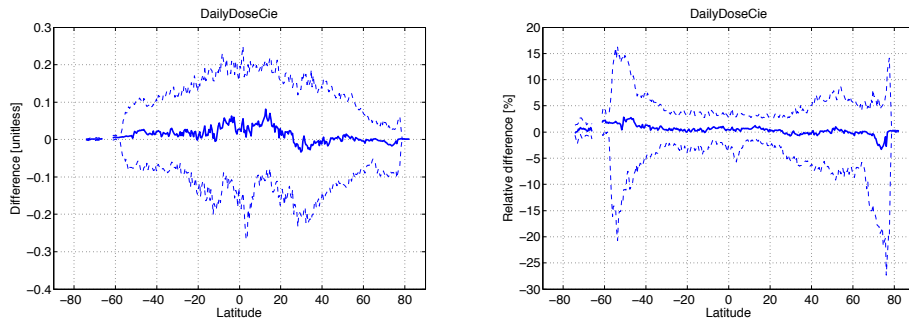


Figure 2.16: Median difference GOME-2B - GOME-2A (left) and relative difference $(\text{GOME-2B} - \text{GOME-2A}) / \text{GOME-2B}$ for CIE weighted daily dose for 10.4.2013 as a function of latitude. Dashed lines show 16th and 84th percentiles of the distribution.

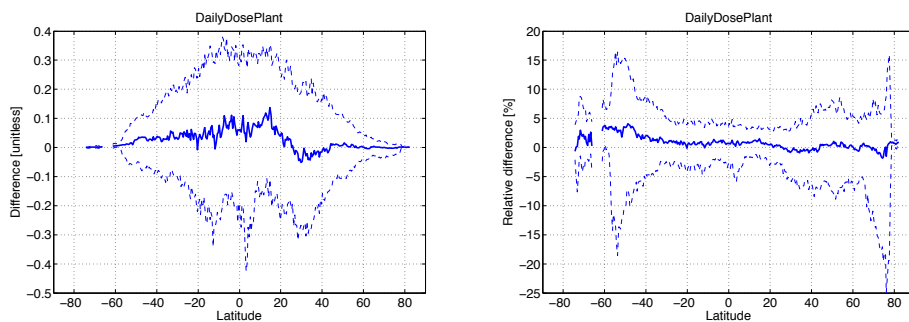


Figure 2.17: Median difference GOME-2B - GOME-2A (left) and relative difference $(\text{GOME-2B} - \text{GOME-2A}) / \text{GOME-2B}$ for plant response weighted daily dose for 10.4.2013 as a function of latitude. Dashed lines show 16th and 84th percentiles of the distribution.

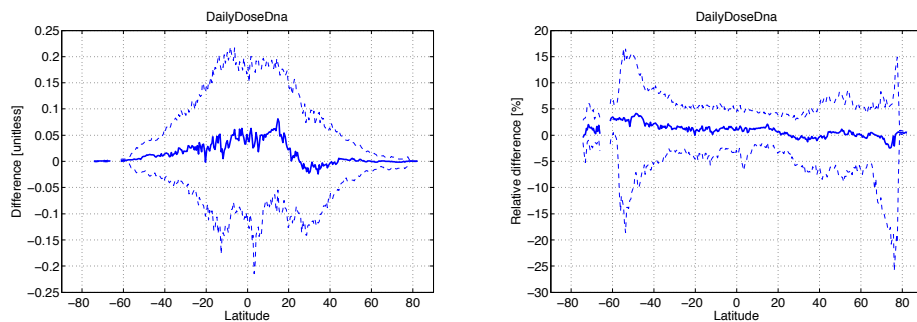


Figure 2.18: Median difference GOME-2B - GOME-2A (left) and relative difference $(\text{GOME-2B} - \text{GOME-2A}) / \text{GOME-2B}$ for DNA damage weighted daily dose for 10.4.2013 as a function of latitude. Dashed lines show 16th and 84th percentiles of the distribution.

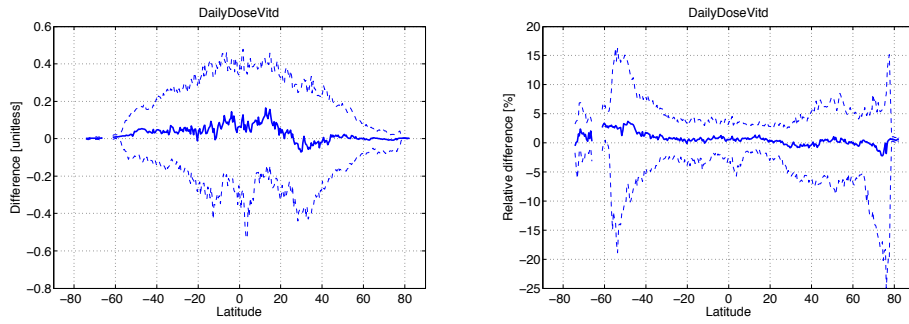


Figure 2.19: Median difference GOME-2B - GOME-2A (left) and relative difference $(\text{GOME-2B} - \text{GOME-2A}) / \text{GOME-2B}$ for vitamin D weighted daily dose for 10.4.2013 as a function of latitude. Dashed lines show 16th and 84th percentiles of the distribution.

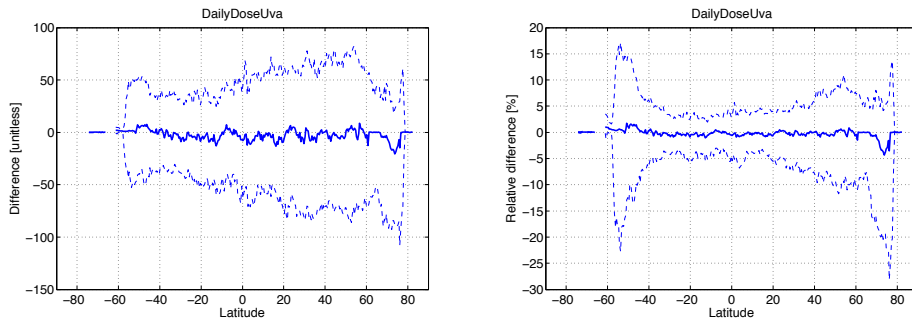


Figure 2.20: Median difference GOME-2B - GOME-2A (left) and relative difference $(\text{GOME-2B} - \text{GOME-2A}) / \text{GOME-2B}$ for UVA weighted daily dose for 10.4.2013 as a function of latitude. Dashed lines show 16th and 84th percentiles of the distribution.

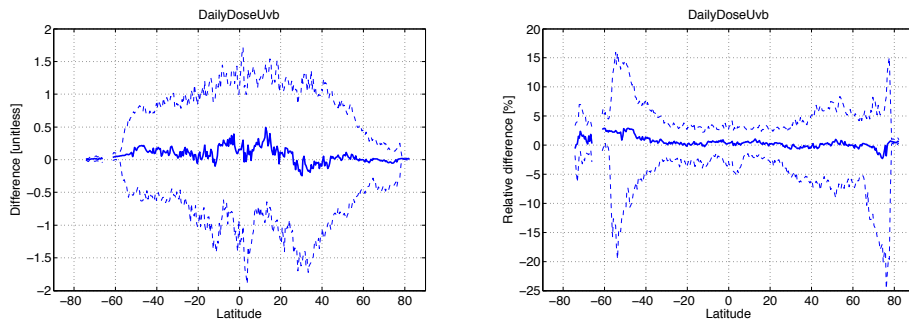


Figure 2.21: Median difference GOME-2B - GOME-2A (left) and relative difference $(\text{GOME-2B} - \text{GOME-2A}) / \text{GOME-2B}$ for UVB weighted daily dose for 10.4.2013 as a function of latitude. Dashed lines show 16th and 84th percentiles of the distribution.

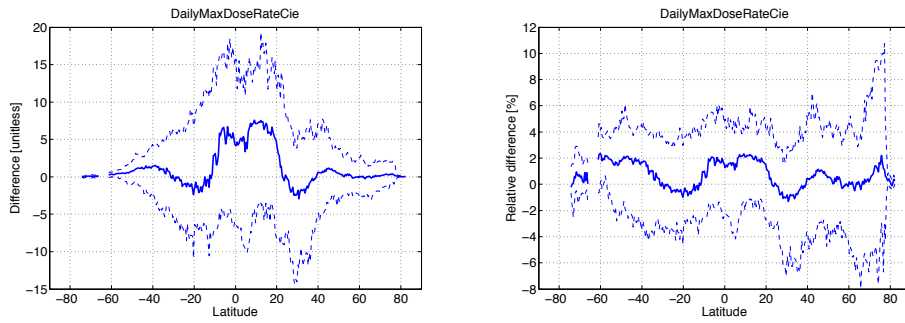


Figure 2.22: Median difference GOME-2B - GOME-2A (left) and relative difference $(\text{GOME-2B} - \text{GOME-2A}) / \text{GOME-2B}$ for CIE weighted daily maximum dose rate for 10.4.2013 as a function of latitude. Dashed lines show 16th and 84th percentiles of the distribution.

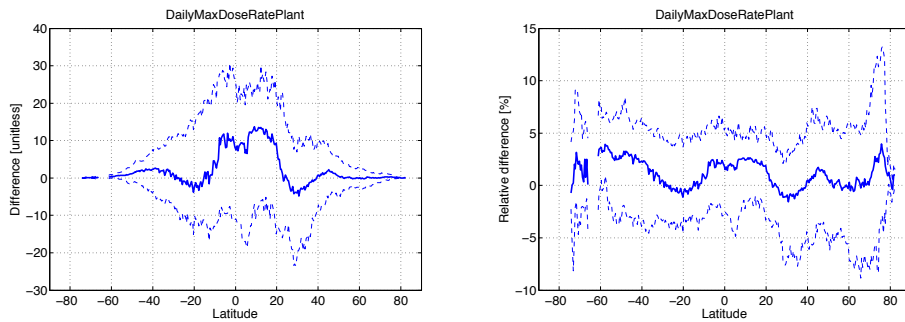


Figure 2.23: Median difference GOME-2B - GOME-2A (left) and relative difference $(\text{GOME-2B} - \text{GOME-2A}) / \text{GOME-2B}$ for plant response weighted daily maximum dose rate for 10.4.2013 as a function of latitude. Dashed lines show 16th and 84th percentiles of the distribution.

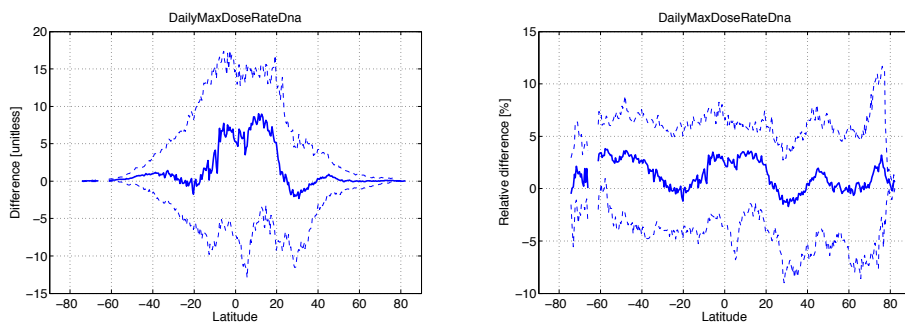


Figure 2.24: Median difference GOME-2B - GOME-2A (left) and relative difference $(\text{GOME-2B} - \text{GOME-2A}) / \text{GOME-2B}$ for CIE weighted daily maximum dose rate for 10.4.2013 as a function of latitude. Dashed lines show 16th and 84th percentiles of the distribution.

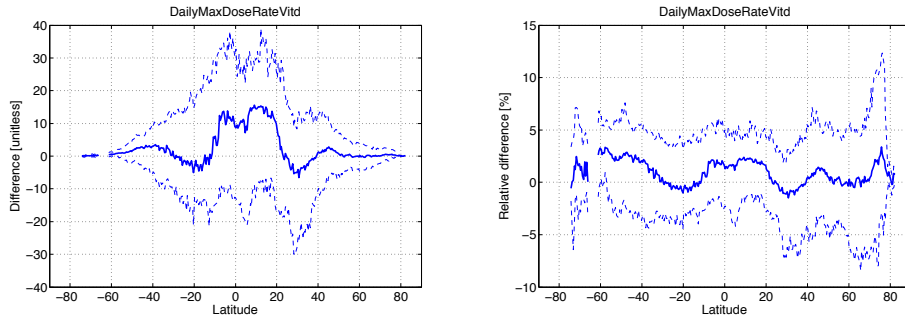


Figure 2.25: Median difference GOME-2B - GOME-2A (left) and relative difference $(\text{GOME-2B} - \text{GOME-2A}) / \text{GOME-2B}$ for vitamin D weighted daily maximum dose rate for 10.4.2013 as a function of latitude. Dashed lines show 16th and 84th percentiles of the distribution.

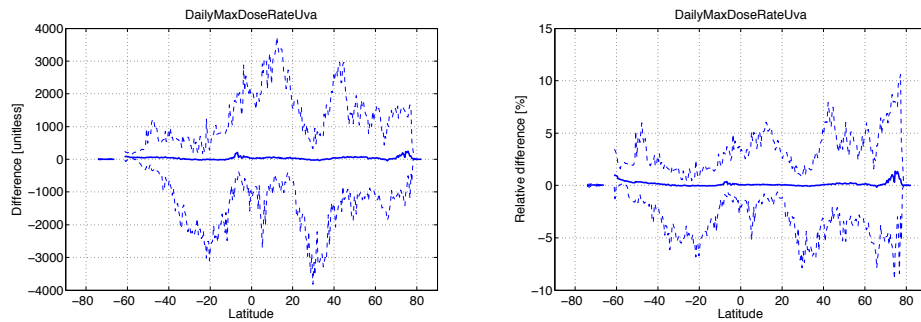


Figure 2.26: Median difference GOME-2B - GOME-2A (left) and relative difference $(\text{GOME-2B} - \text{GOME-2A}) / \text{GOME-2B}$ for UVA weighted daily maximum dose rate for 10.4.2013 as a function of latitude. Dashed lines show 16th and 84th percentiles of the distribution.

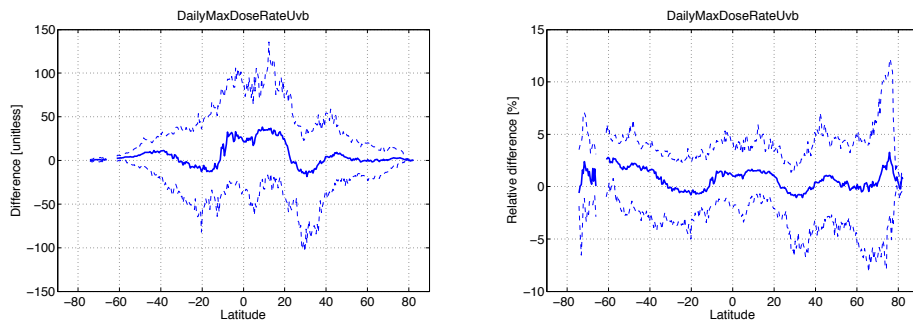


Figure 2.27: Median difference GOME-2B - GOME-2A (left) and relative difference $(\text{GOME-2B} - \text{GOME-2A}) / \text{GOME-2B}$ for UVB weighted daily maximum dose rate for 10.4.2013 as a function of latitude. Dashed lines show 16th and 84th percentiles of the distribution.

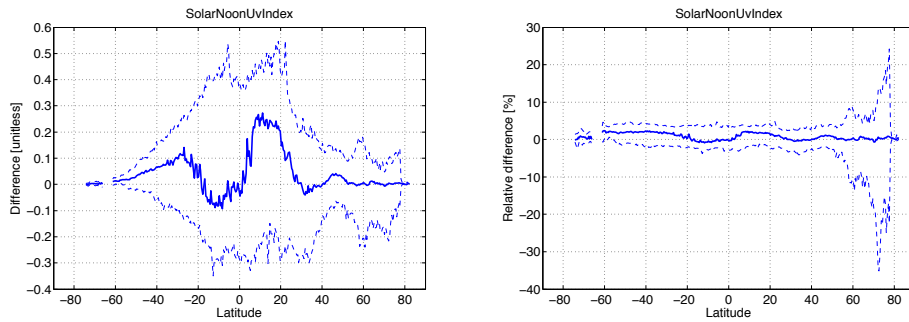


Figure 2.28: Median difference GOME-2B - GOME-2A (left) and relative difference $(\text{GOME-2B} - \text{GOME-2A}) / \text{GOME-2B}$ for solar noon UV index for 10.4.2013 as a function of latitude. Dashed lines show 16th and 84th percentiles of the distribution.

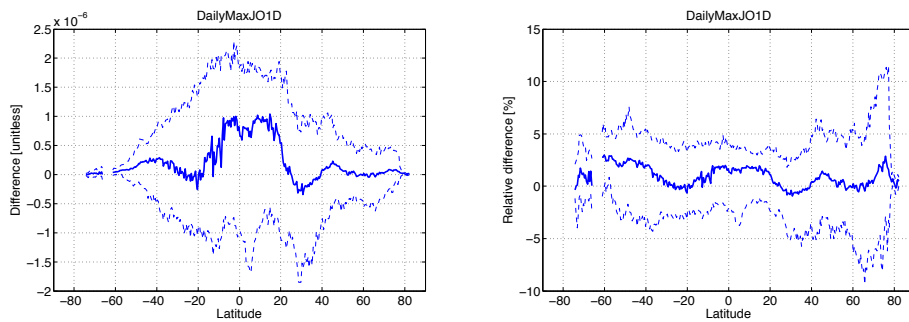


Figure 2.29: Median difference GOME-2B - GOME-2A (left) and relative difference $(\text{GOME-2B} - \text{GOME-2A}) / \text{GOME-2B}$ for daily maximum ozone photolysis rate for 10.4.2013 as a function of latitude. Dashed lines show 16th and 84th percentiles of the distribution.

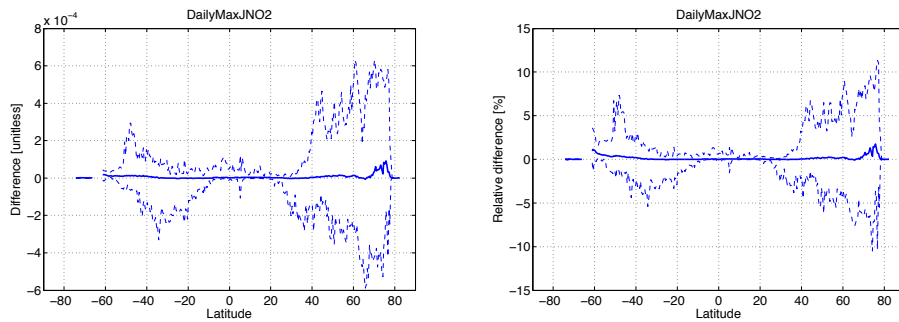


Figure 2.30: Median difference GOME-2B - GOME-2A (left) and relative difference $(\text{GOME-2B} - \text{GOME-2A}) / \text{GOME-2B}$ for daily maximum NO_2 photolysis rate for 10.4.2013 as a function of latitude. Dashed lines show 16th and 84th percentiles of the distribution.

2.2 Photolysis rates

In OUV, the photolysis frequency j_x for a species X is obtained by weighting and integrating over wavelength [AD1]

$$j_x = \int_{\lambda} \sigma_x(\lambda, T) \phi_x(\lambda, T) E_s(\lambda, \theta_0, z) d\lambda \quad (2.1)$$

where $\sigma_x(\lambda, T)$ is the absorption cross-section, $\phi_x(\lambda, T)$ is the photolysis quantum yield for the species X , T is the temperature, z is the height from the surface, and $E_s(\lambda)$ is the spherical spectral irradiance (actinic flux), given by

$$\begin{aligned} E_s(\lambda) &= \int_0^{2\pi} d\phi \int_{-\frac{\pi}{2}}^{\frac{\pi}{2}} L(\lambda, \theta, \phi) \sin\theta d\theta \\ &= \int_0^{2\pi} d\phi \int_0^{\frac{\pi}{2}} L^-(\lambda, \theta, \phi) \sin\theta d\theta + \int_0^{2\pi} d\phi \int_{-\frac{\pi}{2}}^0 L^+(\lambda, \theta, \phi) \sin\theta d\theta \\ &= E_s^-(\lambda) + E_s^+(\lambda) \end{aligned} \quad (2.2)$$

where L^- is the downwelling radiance incident on the upper hemisphere of the detector and L^+ is the upwelling radiance incident on the lower hemisphere of the detector, and $E_s^-(\lambda)$ and $E_s^+(\lambda)$ refer to the corresponding hemispherical spectral irradiances. The OUV product is given at the surface level and the integration of the actinic flux is over the whole sphere, i.e. 4π steradians.

2.2.1 O₃ photolysis rates

GOME-2 test products of daily maximum ozone photolysis rates were compared to measurements for year 2008 from ENEA Station for Climate Observations on the island of Lampedusa, Italy. Metcon DAS instrument on Lampedusa has an actinic radiation input optical system, that is coupled through an optical fiber to a Carl Zeiss spectrometer. A diode array detector measures the actinic radiation between 280 and 700 nm. the instrument is calibrated with 1000 W NIST traceable FEL lambs, using the field calibrator developed at NOAA. 137 matching data points were obtained, between March and September, 2008. Figure 2.31 shows the scatter plot and time series for $j(\text{O}_1\text{D})$. Comparisons show good agreement, with mean bias of 0.1 %, RMS of 15.2 % and r^2 of 0.60.

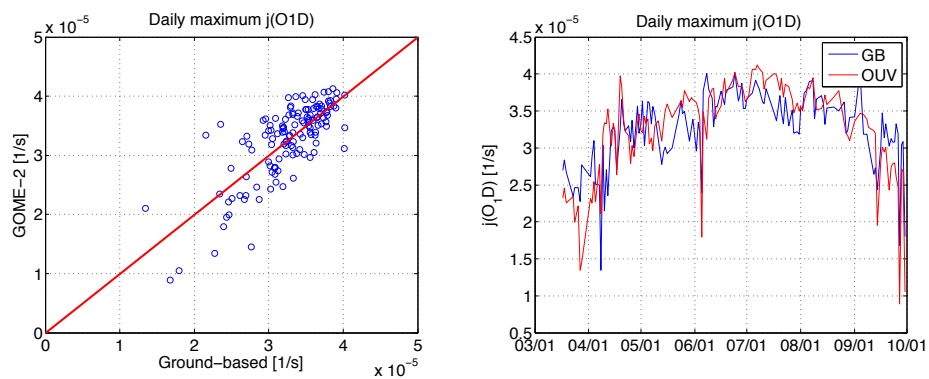


Figure 2.31: Left: scatterplot of $j(\text{O}_1\text{D})$ from GOME-2 and Lampedusa. Right: time series of $j(\text{O}_1\text{D})$ from GOME-2 and Lampedusa.

2.2.2 NO₂ photolysis rates

Overview

The validation of the NO₂ photolysis rate product is hampered by the fact that the ground-based instruments often measure only the downwelling component of the actinic flux incident on the upper hemisphere.

Here, we define the two components of the j_{NO_2} photolysis frequency according to the direction of the hemispherical actinic flux

$$j_{NO_2}^- = \int_{\lambda} \sigma_{NO_2}(\lambda, T) \phi_{NO_2}(\lambda, T) E_s^-(\lambda, \theta_0, z) d\lambda \quad (2.3)$$

for the downwelling component, and

$$j_{NO_2}^+ = \int_{\lambda} \sigma_{NO_2}(\lambda, T) \phi_{NO_2}(\lambda, T) E_s^+(\lambda, \theta_0, z) d\lambda \quad (2.4)$$

for the upwelling component, giving for the total photolysis frequency

$$j_{NO_2} = j_{NO_2}^- + j_{NO_2}^+ \quad (2.5)$$

Figure 2.32 shows two different ground-based instruments made by Metcon Inc. The 4π filter radiometer measures the j_{NO_2} weighted actinic flux for the upper and lower hemispheres simultaneously with two hemispherical detectors. The filters are designed to provide the weighting required by eq. 2.1. The values for the two hemispheres, i.e. $j_{NO_2}^-$ and $j_{NO_2}^+$, can be studied separately. On the other hand, the 2π diode array spectrograph measures only the downwelling spectral actinic flux incident on the upper hemisphere, $E_s^-(\lambda)$. This is converted to $j_{NO_2}^-$ values in a post-processing step according to eq. 2.3.

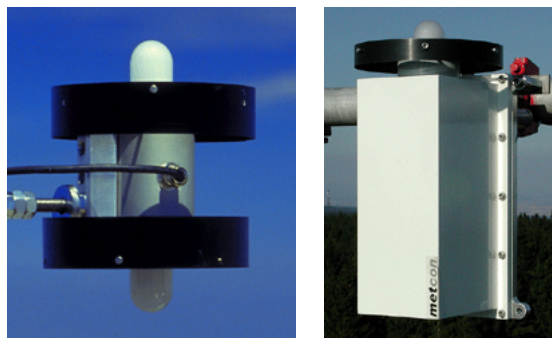


Figure 2.32: Metcon 4π j_{NO_2} filter radiometer (left) and 2π diode array spectrograph (right). From <http://website.metcon-us.com>.

The downwelling component of the j_{NO_2} is less sensitive to the local surface albedo below the instrument than the value for the full sphere. This is one reason why the ground-based measurement teams avoid measuring the upwelling component. Figure 2.33 (left)

shows the dependence of the surface level j_{NO_2} and its components on the surface albedo for different solar zenith angles in a typical cloud-free atmosphere. Figure 2.33 (right) shows the same dependence for the $j_{NO_2}^-/j_{NO_2}$ ratio. At zero surface albedo the upwelling component $j_{NO_2}^+$ is practically zero, and the total is equal to the downwelling component. The fraction of the upwelling component increases strongly with surface albedo. At 0.2 surface albedo and 40 degrees solar zenith angle the downwelling component is about 80 % of the total. Clearly, the strong dependence of the upwelling component on the surface albedo causes a representativeness error between the ground-based and satellite measurements.

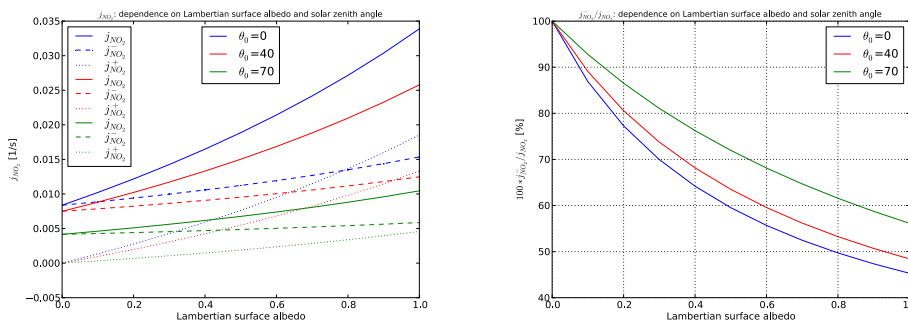


Figure 2.33: Left: the dependence of the surface level j_{NO_2} , $j_{NO_2}^-$ and $j_{NO_2}^+$ on the surface albedo for different solar zenith angles in a typical clear-sky atmosphere. Right: the same dependence for $j_{NO_2}^-/j_{NO_2}$ ratio.

Comparison with CARES campaign measurements

The Carbonaceous Aerosols and Radiative Effects Study (CARES) was organized by The Atmospheric Radiation Measurement (ARM) Climate Research Facility in the central California region in June 2010 (campaign.arm.gov/cares/). The main goal was to study the evolution of black carbon and secondary organic aerosols from both urban/manmade and biogenic sources. A multitude of measurements were performed to support the aerosol study including j_{NO_2} and actinic flux measurements. Here, we compare these ground-based measurements with the corresponding OUV j_{NO_2} product. The ground-based measurements were performed on two sites as depicted in figure 2.34.

The 'T0' site is located within the Sacramento urban source area (on the campus of American River College), which is about 14 km to the northeast of the Sacramento downtown area. At this site, the j_{NO_2} values were measured with a 4π radiometer. The exact specifications of the instrument were not found but it is assumed to be a 4π version of the Metcon filter radiometer shown in figure 2.32 (left), or similar. The data files contain both $j_{NO_2}^-$ and $j_{NO_2}^+$ (in our notation) components. This allows estimation of the surface albedo contributions shown in figure 2.33.

The 'T1' site is located in the downwind area about 40 km further to the northeast at

the K-8 Northside School in Cool, California. At this site, the $j_{NO_2}^-$ values were computed from the downwelling hemispherical actinic flux spectra measured with a diode-array spectrometer, assumed to be a Metcon 2π spectrograph shown in figure 2.32 (right), or similar. Diurnal j_{NO_2} data for representative days at the T0 site are plotted in figure 2.35.



Figure 2.34: Locations of the T0 and T1 sites in the CARES campaign (from [RD1]).

On the afternoon of 19 June the response of the instrument suddenly jumps up. The values for the following day 20 June are suspiciously large. The values are still too large on the 21 June until the response drops to normal level in the afternoon. Therefore, the values for 19, 20 and 21 June at the T0 site were classified as bad.

Figure 2.36 compares the daily maximum surface level j_{NO_2} values of the OUV product with the daily maximum $j_{NO_2}^-$ and j_{NO_2} values for the T0 site, together with the daily maximum $j_{NO_2}^-$ values for the T1 site. The OUV j_{NO_2} values agree well with the ground-based $j_{NO_2}^-$ values for both sites while the j_{NO_2} values for the T0 site are significantly larger than the OUV values. Both sites are covered by the same OUV grid cell, and the average albedo used for this grid cell was 0.02 for the whole period. From figure 2.36 we estimate the $j_{NO_2}^-/j_{NO_2}$ ratio to be about 0.8 at the T0 site. The noon solar zenith angle was about 15 degrees for the days of the campaign. From figure 2.33 (right) we obtain a value of 0.2 for the surface albedo under the instrument. The difference in the surface albedos gives a representativeness error of ca. 20 %. Because the surface albedo used for the OUV product is close to zero, the ground-based $j_{NO_2}^-$ values represent well the OUV values. The $j_{NO_2}^-$ values for both sites are within 20 % limits of the OUV product.

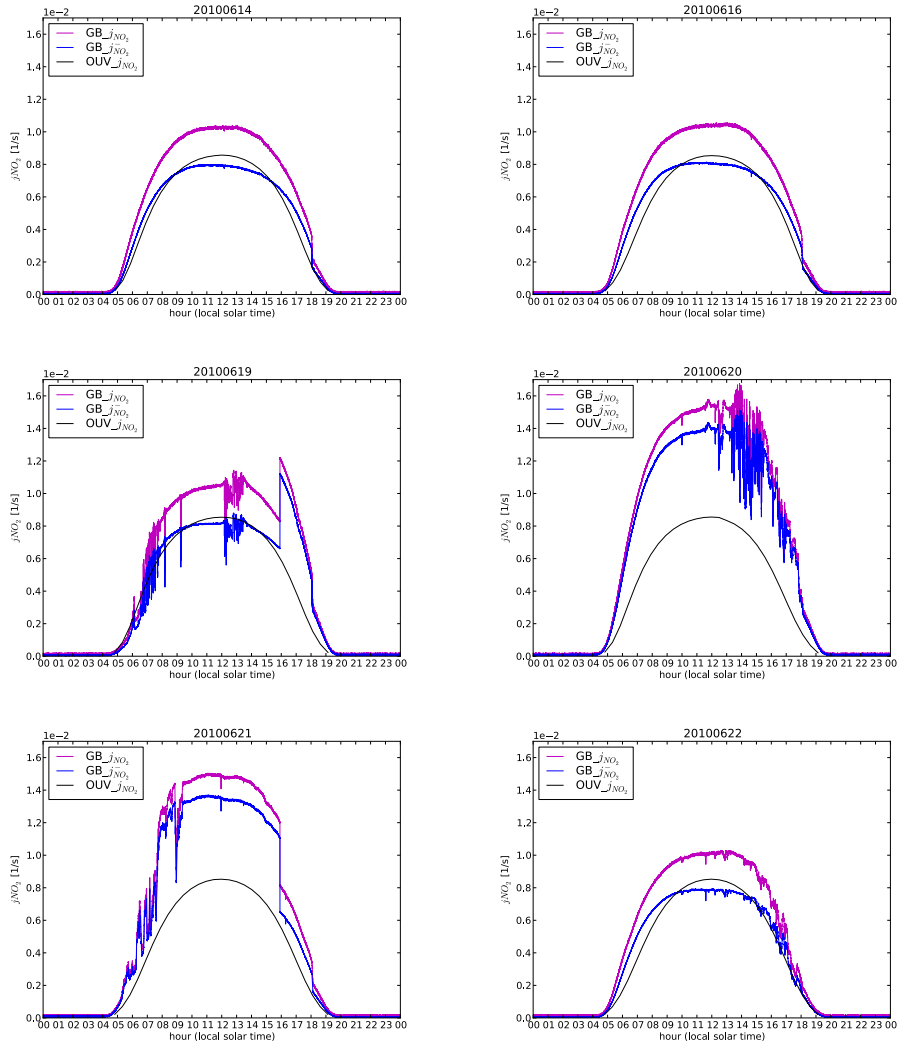


Figure 2.35: Examples of daily comparisons of OUV j_{NO_2} values (black) with corresponding j_{NO_2} (magenta) and \bar{j}_{NO_2} (blue) values for the T0 site data. The ground-based data for 19, 20 and 21 June are considered as bad quality because of the apparent jump in the response of the instrument from the afternoon of 19 June until the afternoon of 21 June. For the other days, the OUV j_{NO_2} values agree well with the ground-based \bar{j}_{NO_2} values as explained in the text. Since no quality flags were included in the ground-based data, days with unphysical jumps were labeled "bad" by visual inspection. Reason for the jumps is not clear from the documentation of the ground-based data.

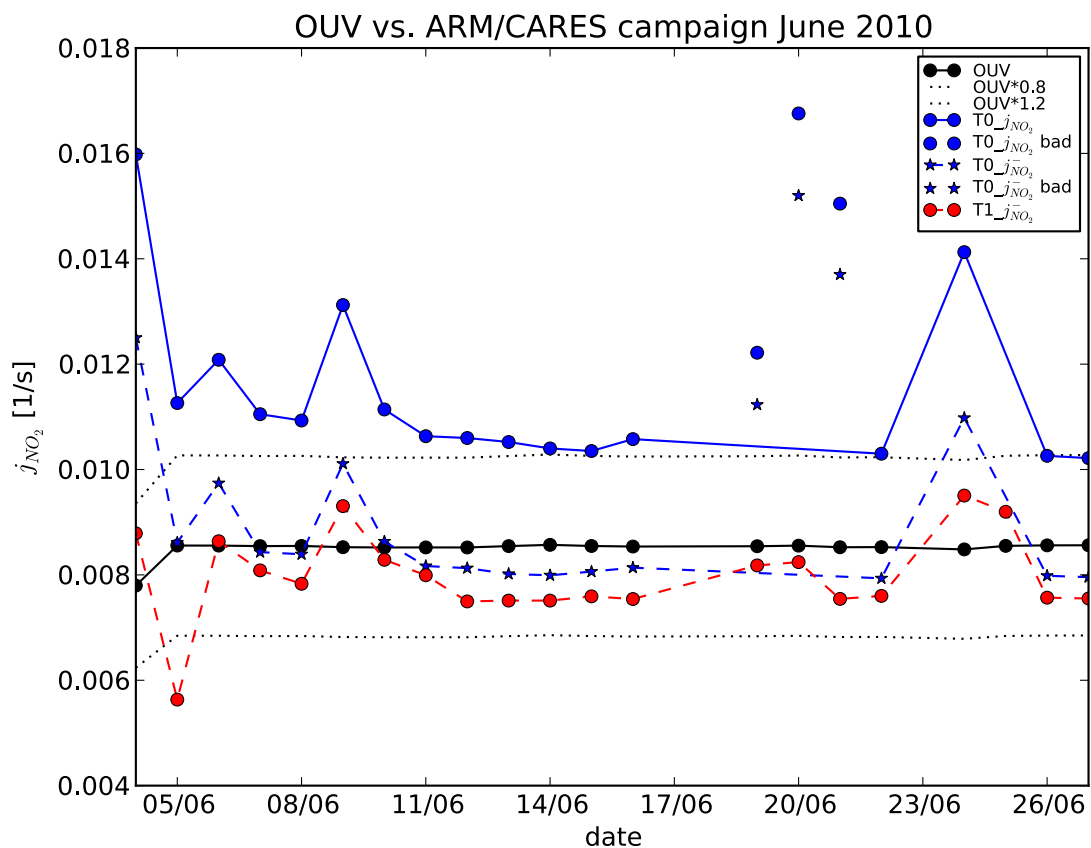


Figure 2.36: Time series of OUV j_{NO_2} values (black) with corresponding j_{NO_2} values for the T0 site (blue solid circles), $j_{NO_2}^-$ for the T0 site (blue stars) and $j_{NO_2}^-$ for the T1 site (red solid circles). The ground-based data points considered as good quality are connected with solid or dashed lines to guide the eye. The values at the T0 site between 19 and 21 June are considered as bad quality as explained in the text. The ground-based $j_{NO_2}^-$ values are within the 20 % error limits of the OUV values (black dotted lines).

2.3 Vitamin D weighting function

Vitamin D weighting product was compared to Brewer observations from Jokioinen and Sodankyla from June 2007 to April 2013. Scatter plots 2.32 and 2.33 show comparisons of D-vitamin weighted daily doses and daily maximum dose rates between GOME-2 and Brewer at Jokioinen and Sodankyla, respectively. Correlation is good for all comparisons (0.97 and 0.93 for Jokioinen, 0.96 and 0.94 for Sodankyla). Daily doses show small positive median relative difference (6.2 % for Jokioinen and 6.0 % for Sodankyla) and daily maximum dose rates small negative median relative difference (-2.7 % for Jokioinen and -3.7 % for Sodankyla).

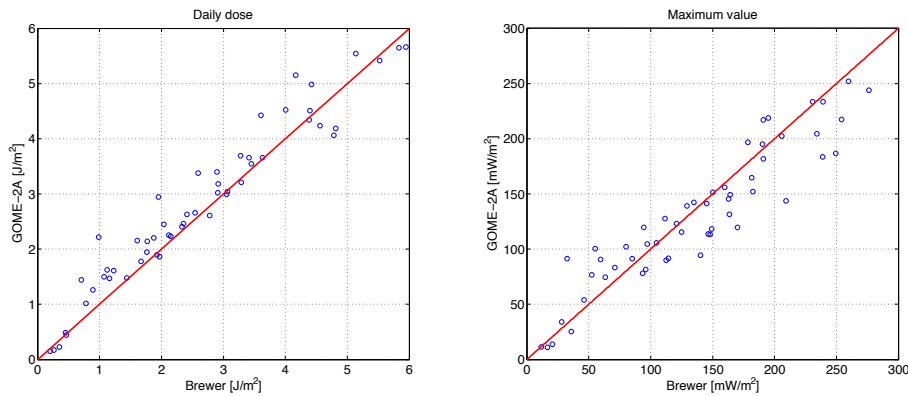


Figure 2.37: Scatterplots of daily doses (left) and daily maxima (right) of vitamin D weighted irradiance from GOME-2 and Jokioinen.

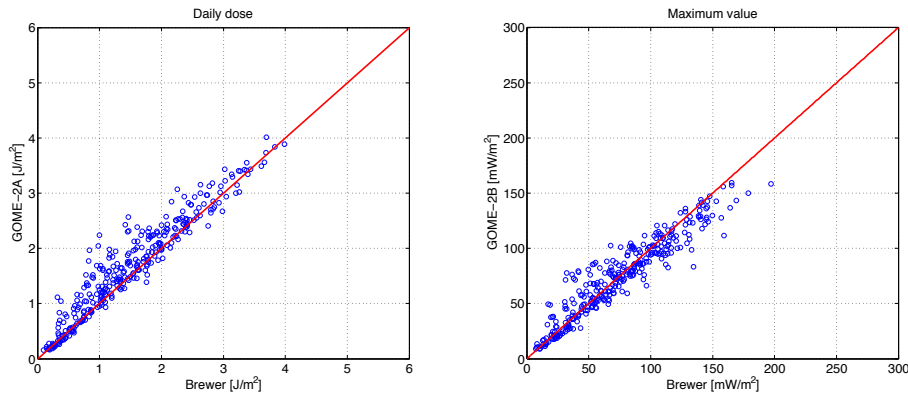


Figure 2.38: Scatterplots of daily doses (left) and daily maxima (right) of vitamin D weighted irradiance from GOME-2 and Sodankyla.

Chapter 3

Conclusions

GOME-2B CIE daily dose shows good agreement with GOME-2A, with median difference of less than 3 % in almost all latitudes. Cyclical differences between instruments are observed in various products, but differences are generally within expected range.

O₃ photolysis rates are in good agreement with with ground-based observations with daily doses showing 6 % positive median relative difference and maximum dose rates showing 3-4 % negative median relative difference.

NO₂ photolysis rates are in good agreement (within 20 % limits of the OUV product) with ground-based $j_{NO_2}^-$ observations from both sites of CARES campaign measurements. $j_{NO_2}^+$ observations from site T0, however are significantly higher than OUV photolysis rates.

D-vitamin weighted OUV products show very good correlation with Brewer observations. Comparisons of daily doses show small positive (6.2 % and 6.0 %) and comparisons of daily maximum dose rates small negative (-2.7 % and -3.7 %) biases.